Parametric analysis of the dynamic elastic response of composite hydrofoils and airfoils

Deniz Tolga Akcabay, Yin Lu Young

University of Michigan, Department of Naval Architecture and Marine Engineering, Ann Arbor, MI, U.S.A.

ABSTRACT

Lightweight and high strength composites are attractive as alternatives to metal alloys for lifting devices such as marine propulsors. However, most of the work thus far focus on the steady-state response. The objective of this work is to study the impact of various nondimensional parameters on the dynamic hydroelastic response of composite foils. The results show that if the principal directions of the fibers are oriented moderately toward the leading edge, static-divergence instability is avoided, but flutter instability may become critical. For hydrofoils, a new mode appears (due to the nonlinear wake effects) with very low frequency at some high speed, and the damping of the new mode may go to zero at a critical higher speed. In contrast, for airfoils, it is one of the original structural modes that loses its damping during flutter. Typical flow-induced damping values are higher, and the natural frequencies are lower, in water than in air. As the aspect ratio of the foils decrease, the fluid loads decrease, warping effects become more significant, and the critical speeds for the onset of elastic instabilities become higher. Lowering the thickness to chord ratio lowers the dimensional structural stiffness, natural frequencies and divergence speed, but the non-dimensional results remain unchanged, as the fluid and plate models omit plate thickness effects and a linear stress gradient is assumed across the thickness of the plate.

Keywords: Composite; dynamics; stability; static-divergence; flutter

1. INTRODUCTION

High-strength, lightweight composite materials with high resistance to corrosion and fatigue have been commissioned during the last few decades for aerospace and ground vehicles, as well as for wind turbines. There have been many studies on their aeroelastic response, interested readers may refer to: (Mihaila-Andres et al 2016) (Farsadi & Hasbestan 2017) (Botelho et al 2006) (Edwards & Wieseman 2008) (Lottati 1985) (Shirk et al 1986) (Weisshaar & Foist 1985) (Weisshaar 1981) (Weisshaar 1980) (Minguet 1989). A particular application of composite structures are their use for various lift generating surfaces, such as wings, rudders, ailerons, propeller and turbine blades, etc., which are essentially cantilevered plates. Depending on their customizable lay out, composite structures could exhibit specific material anisotropies. For instance, cantilevered plates have various bending and twisting degrees of freedom, and the anisotropic response of composite materials could be exploited to improve performance. As suggested by their name, the purpose of lifting surfaces is to generate lift. Until flow separation develops, lift increases proportional to their effective angle-of-attack (AoA), but when the AoA reaches the stall angle, the lift drops and the drag increases rapidly. Even prior to stall, the hydrodynamic lift and moment relative to the elastic axis can lead to elastic deformations that can modify the hydrodynamic loads, depending on the structural stiffness. Furthermore, flutter and static-divergence instabilities may occur as the external forces may negate the total effective stiffness and damping of the lifting surface. Note that there exist non-traditional applications of lifting surfaces, where they are designed to undergo flow-induced vibrations or flutter for flow kinetic energy harvesting purposes (e.g. (Akcabay & Young 2012a), (Akcabay & Young 2012b), (Erturk & Inman 2011)).

In contrast to the vast aerospace applications, composites are still not frequently used for marine applications. This is in part because of the challenge with the design of marine composites and the lack of systematic experimental data. The fluid forces acting on the marine structures are higher than the same structure in air operating at the same speed, as these forces are proportional to the fluid density, and the density of seawater is about 850 times higher than air. In addition, high-speed operations near the sea-surface may be susceptible to cavitation and ventilation, which can lead to sudden and drastic load changes, as well as flow-induced vibrations, related instability and control issues

(Young et al 2017). While most aerospace structures tend to employ hollow or foam core geometries to reduce weight and to embed various sensors/actuators to achieve multifunctional structures, the stringent strength requirements and the harsh sea environments typically force hydrodynamic lifting devices have solid/non-hollow profiles (Young et al 2016). (Lin 1996), (Lee & Lin 2004), (Young 2008) are among the first studies that considered the hydroelastic response of composite marine propellers. The recent review article by (Young et al 2016) summarizes the current state-of-art of composite marine propulsors and turbines. The recent works of (Zarruk et al 2014), (Young et al 2018), and (Liao et al 2019) show the steady-state hydroelastic response of composite hydrofoils. They show that by taking advantage of the intrinsic bend-twist coupling properties of anisotropic composites, hydrofoils can be designed to undergo nose-down deformations that are proportional to the load, and hence flow separation, cavitation, and the onset of static-divergence instabilities could be delayed. Recall that static-divergence occurs when the effective structural torsion stiffness is totally negated by the fluid de-stiffening effects.

In addition to higher fluid forces and lower operating speeds in water, (Besch & Liu 1974) showed that the hydroelastic response of submerged structures can exhibit surprising differences than their counterparts in air. Specifically, they experimentally and theoretically showed that a new vibration mode with very low frequency might appear for hydrofoils operating above a certain operating speed. Depending on the operating condition, this new mode may eventually lose its damping and reach flutter instability, which results in increasing load fluctuations and vibration in the presence of negative total damping. The emergence of such a new mode could be critical for structural designs, as a low frequency mode without sufficient damping can easily interact with various ambient excitation sources (e.g. sea state excitations in marine environments or non-uniform wake inflow due to hull-propeller-rudder interactions). In (Akcabay & Young 2019), we have numerically showed that, indeed, such a new mode may appear for a cantilevered composite foil/plate in water if there is a positive coupling between the nose-up twist and bend-up deformations. Note that the wake of the flow past the cantilevered foil undergoing unsteady spanwise bending and twisting deformations exerts nonlinear convolution terms in the hydrodynamic forces, affecting the elastic response of the hydrofoil, which in turn permits the emergence of the new mode. Our same work also showed that the dynamic-to-static load ratios could be significantly higher for composite lifting surfaces operating in water compared to in air.

The objective of this study is to examine how various critical non-dimensional parameters affect the dynamic hydroelastic response of composite lifting surfaces. To focus on the physics, a simple cantilevered plate configuration is used as a canonical proxy to more complex lifting surfaces such as propellers, turbines, and energy saving devices. The focus is on the dynamic hydroelastic response, as parametric studies of the steady-state response have already been discussed in previous work by the authors (see (Young et al 2016) for a recent review). It should be noted that the current work does not consider free surface and cavitation effects. We also assume compressibility and viscous effects are negligible, so potential flow assumptions are assumed to be valid.

The organization of this paper is as follows: Section 2 describes the geometry, the problem setup, and the critical nondimensional parameters. Section 3 outlines how the hydroelastic response of a cantilevered composite plate changes with the nondimensional parameters. Section 4 lists our conclusions and future works.

2. PROBLEM DESCRIPTION: GEOMETRY, PHYSICAL AND NUMERICAL MODELS

As explained in more detail in (Akcabay & Young 2019), we model a cantilever composite plate in external fluid flow with spanwise bending and twisting degrees of freedom. The model that we study is shown in Fig. 1a, where L is the length (span) of the plate, $2b$ is the width (chord), q is the thickness, and θ is the effective angle of the fibers of the composite material relative to the spanwise axis, and defined positive when leaning towards the leading edge. Here, we model the composite plate with an equivalent unidirectional ply made of a matrix/resin material reinforced with strong fibers. In practice, the composite material may consist of many layers of laminated plies with variable fiber angles and stacking sequences. However, was shown in (Kramer & Young 2013) and (Gay & Hoa 2007), the load-dependent deformation response of such a structure may be modelled with an equivalent single layer, where the fibers make an effective angle θ with respect to the spanwise axis.

$h(y,t)$ and $\psi(y,t)$ are used to denote the spanwise bending and twisting deformations, respectively, defined at the elastic axis, and t is time. The Cartesian coordinates x-y-z are chosen such that x is parallel to the incoming flow, y is along the plate length, and z is such that $z = x \times y$. U_0 in Fig. 1a is the speed of the incoming fluid flow. Fig. 1b is a cross-sectional view of the plate (normal to the y-axis) that shows the definitions of various critical length scales used in the physical model. These length parameters are: ab, the distance from the mid-chord of the section (where x=0) to the elastic axis (E.A.), which is positive if E.A. is aft of the midpoint; $x_\alpha b$, the distance from the E.A. to the center-of-gravity (C.G.) of the section, which is positive if C.G. is aft of the E.A.; and eb is the distance from the E.A. to the center of pressure (C.P.), which is positive if C.P. is upstream of the E.A. The C.P. is the location where the resultant lift force (F_z^{fluid}) acts, and for most cases where eb is positive, the lift-force induces a bending up and nose-up deformation about the E.A. Finally, in Fig. 1b, α_0 is the initial angle-of-attack (AoA) of the plate with respect to the inflow.

As we have done in (Akcabay & Young 2019), we model the plate with linear beam equations with bend-twist coupling term (K_s) that arises due to the fiber orientation in the plate, and with warping stiffness (S_s). The equations of this model are given in Eqns. (1) and (2):

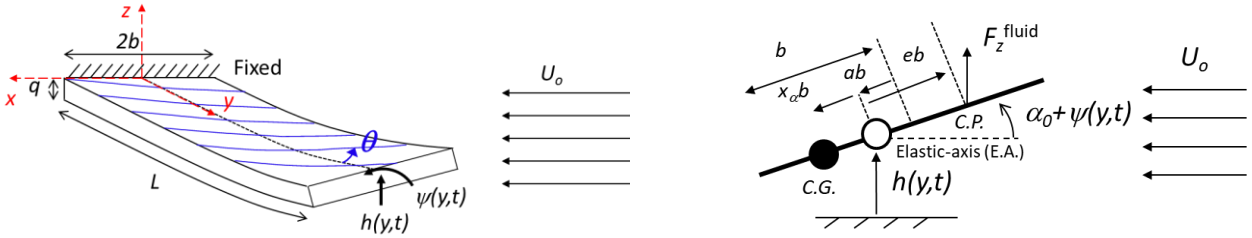

Figure 1: A cantilevered composite plate with bending and twisting degrees of freedom with length *L*, width *2b*, and thickness *q* in cross flow along the *x*-axis with a speed U_0. The composite plate is made of unidirectional fibers that are aligned with an angle θ with respect to the *y*-axis along the plate length towards the leading edge of the plate. The initial angle of attack is α_0, and various length scales are defined in the plot (b). Plot (a) is the 3D view, plot (b) is the cross-sectional view normal to the *y*-direction. C.P. is the center of pressure, where the resultant lift force, F_z^{fluid}, acts and C.G. is the sectional center-of-gravity.

$$\begin{aligned} & m_s \frac{\partial^2 h}{\partial t^2} - m_s x_\alpha b \frac{\partial^2 \psi}{\partial t^2} \\ & = -EI_s \frac{\partial^4 h}{\partial y^4} - K_s \frac{\partial^3 \psi}{\partial y^3} - ab \frac{\partial^4 \psi}{\partial y^4} + F_z^{fluid} \end{aligned}, \quad (1)$$

$$\begin{aligned} & I_s^{E.A.} \frac{\partial^2 \psi}{\partial t^2} - m_s x_\alpha b \frac{\partial^2 h}{\partial t^2} \\ & = GJ_s \frac{\partial^2 \psi}{\partial y^2} + K_s \frac{\partial^3 h}{\partial y^3} - abEI_s \frac{\partial^4 h}{\partial y^4} - S_s \frac{\partial^4 \psi}{\partial y^4} + M_y^{fluid} \end{aligned}. \quad (2)$$

In Eqns. (1) and (2), m_s is the sectional mass of the plate, $I_s^{E.A.}$ is the sectional mass moment of inertia of the plate about the E.A., EI_s and GJ_s are the sectional structural bending and torsion stiffness, and M_y^{fluid} is the sectional fluid induced moment about the E.A.. We neglect gravity and all the other external forces in this model, and we assume uniform inflow. The boundary conditions of this higher-order beam equations are given in Eqns. (3-7).

$$h\big|_{y=0} = 0, \quad \psi\big|_{y=0} = 0, \quad \left.\frac{\partial h}{\partial y}\right|_{y=0} = 0, \quad \left.\frac{\partial \psi}{\partial y}\right|_{y=0} = 0, \quad (3)$$

$$EI_s \left.\frac{\partial^3 h}{\partial y^3}\right|_{y=L} + K_s \left.\frac{\partial^2 \psi}{\partial y^2}\right|_{y=L} + abEI_s \left.\frac{\partial^3 h}{\partial y^3}\right|_{y=L} = 0, \quad (4)$$

$$EI_s \left.\frac{\partial^2 h}{\partial y^2}\right|_{y=L} + K_s \left.\frac{\partial \psi}{\partial y}\right|_{y=L} + abEI_s \left.\frac{\partial^2 \psi}{\partial y^2}\right|_{y=L} = 0, \quad (5)$$

$$GJ_s \left.\frac{\partial \psi}{\partial y}\right|_{y=L} + K_s \left.\frac{\partial^2 h}{\partial y^2}\right|_{y=L} - abEI_s \left.\frac{\partial^3 h}{\partial y^3}\right|_{y=L} - S_s \left.\frac{\partial^3 \psi}{\partial y^3}\right|_{y=L} = 0, \quad (6)$$

$$S_s \left.\frac{\partial^2 \psi}{\partial y^2}\right|_{y=L} + abEI_s \left.\frac{\partial^2 h}{\partial y^2}\right|_{y=L} + abK_s \left.\frac{\partial \psi}{\partial y}\right|_{y=L} = 0. \quad (7)$$

The fluid forces and moments are calculated through Eqns. (8-9), which were originally derived in (Theodorsen 1935), (Sears 1941) for 2-D unsteady forces on a thin plate undergoing harmonic heave and pitch oscillations, similar to the geometry shown Fig. 1b. We applied the steady state lifting line solution of (Glauert 1947) with the 3-D unsteady corrections introduced by (Yates Jr. 1966) to extend Theodorsen's 2-D theory to account for spanwise variations. The method assumes the flow to be incompressible and inviscid, and to be tangential to the plate on both its top and bottom surfaces; and a thin wake sheet being shed from the foil trailing edge in a direction parallel to the inflow. In Eqns. (8-9), ρ_f is the fluid density. The reduction in the 3-D lift slope, a_0, due to induced downwash velocity caused by free vortices shed in the wake is shown in Fig. 2.

$$\begin{aligned} F_z^{fluid} = & -\pi\rho_f b^2 \frac{\partial^2 h}{\partial t^2} - \pi\rho_f b^2 ab \frac{\partial^2 \psi}{\partial t^2} \\ & - \tfrac{1}{2}\rho_f U_0 a_0 2b\Omega(k) \frac{\partial h}{\partial t} \\ & + \tfrac{1}{2}\rho_f U_0 b^2 \left[2\pi + a_0[1-2a]\Omega(k)\right] \frac{\partial \psi}{\partial t} \\ & + \tfrac{1}{2}\rho_f U_0^2 a_0 2b\Omega(k)\left[\psi + \alpha_0\right] \end{aligned}, \quad (8)$$

$$\begin{aligned} M_y^{fluid} = & -\pi\rho_f b^2 ab \frac{\partial^2 h}{\partial t^2} - \pi\rho_f b^4 \left[\tfrac{1}{8} + a^2\right] \frac{\partial^2 \psi}{\partial t^2} \\ & - \tfrac{1}{2}\rho_f U_0 a_0 [eb] 2b\Omega(k) \frac{\partial h}{\partial t} \\ & - \tfrac{1}{2}\rho_f U_0 \frac{b^2}{2}[1-2a]\left[2\pi b - a_0 2eb\Omega(k)\right] \frac{\partial \psi}{\partial t} \\ & + \tfrac{1}{2}\rho_f U_0^2 a_0 [eb] 2b\Omega(k)\left[\psi + \alpha_0\right]. \end{aligned} \quad (9)$$

In Eqns. (8-9),

$$k = \frac{\omega b}{U_0}; \quad \Omega(k) = \frac{H_1^2(k)}{H_1^2(k) + iH_0^2(k)}, \quad (10)$$

where ω is the oscillation frequency of the spanwise bending and twisting deformations.

This work considers the spanwise bending and twisting deformations only. Since the deformations are assumed to be harmonic, we express them as:

$$\begin{pmatrix} h(y,t) \\ \psi(y,t) \end{pmatrix} = \begin{pmatrix} H(y,\omega) \\ \Psi(y,\omega) \end{pmatrix} \exp(i\omega t) \ . \quad (11)$$

Finally, $H_1^2(k)$ and $H_0^2(k)$ in Eqn. (10) are Bessel functions of third kind. In this study, we assume $eb=(1/2+a)b$, so that the center of pressure is at quarter chord aft of the plate's leading edge.

For steady-state analysis, we omit the time-derivative terms in the above equation of motions and take $k=0$ and use $\Omega=1$, and solve for the resultant deformations as a function of α_0 and U_0. For dynamic problems, we predict ω by solving an eigenvalue problem. The numerical procedure for predicting the eigenvalues follows the method described in (Beaulieu & Noiseux 1981) in conjunction with the Secant's method.

The physical and numerical models described above have been validated in (Akcabay & Young 2019) (Akcabay & Young 2018) by comparing the predictions against published results. Specifically, the composite plate aeroelastic predictions matched closely with the reported results in (Edwards & Wieseman 2008), (Lottati 1985). These validations are not repeated here for brevity.

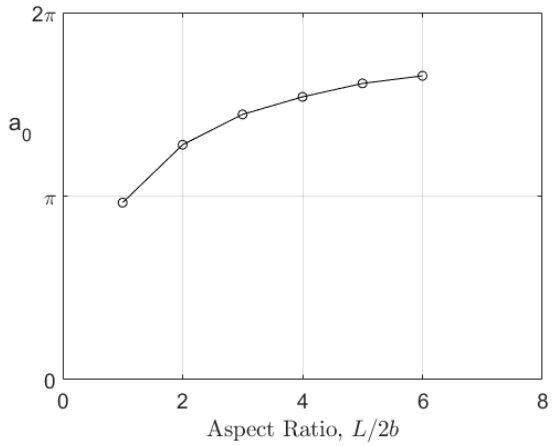

Figure 2: The effect of the aspect ratio *L/2b* on the slope of the 3-D lift coefficient a_0 at steady-state hydroelastic analysis of a rigid hydrofoil.

The key physical parameters that govern the response are: θ (the fiber angle); L, $2b$, q, ab, $x_\alpha b$, eb (the various length scales relating to the plate); EI_s, GJ_s, K_s, S_s (the effective stiffness parameters of the composite plate); m_s, $I_s^{E.A.}$ (the sectional mass and mass moment of inertia of the plate); and U_0, ρ_f (the flow parameters).

For rectangular slender plates, $S_s = EI_s b^2\left(a^2+1/3\right)$ (Lottati 1985). In addition, K_s could be expressed as a function of the EI_s, GJ_s, and θ; and $I_s^{E.A.}$ is just a function of m_s and the sectional geometry of the plate. Hence, the governing independent parameters are:

$$\left\{\theta, L, 2b, q, a, x_\alpha, e, EI_s, GJ_s, m_s, U_0, \rho_f\right\}.$$

These 12 parameters have dimensions of length, time, and mass. Hence, the Buckingham PI theorem yields only 12-3=9 independent nondimensional parameters that can uniquely describe the physical model, which are listed in Table 1 with their physical meanings. Note that the current list of dimensionless parameters do not include the ubiquitous Reynolds (Re), Froude (Fr), and cavitation (σ_v) numbers, as those effects are ignored in our model. In the presence of Re and Fr effects, it is often difficult to design a model scale experiment where all the nondimensional parameters are kept the same between the model and the full-scale, unless the length scale ratio is one. This is because it is impossible to satisfy Re and Fr similarities simultaneously unless the length scale ratio is one. In addition, it may not be possible to find a material that ensure all the nondimensional parameters listed in Table 1 to be the same between the model and full-scale for very small scale models [(Motley & Young 2012), (Akcabay & Young, 2012b), (Ducoin & Young 2013)].

A closer look at the nondimensional parameters listed in Table 1 reveals that the total number of independent variables could be further reduced. First, note that for a rectangular plate, as shown in Fig. 1a, the 2nd moment of area, I_s, and polar moment of area J_s are expressed as:

$$I_s = \frac{2bq^3}{12}, \quad \text{and} \quad J_s = 2bq\frac{q^2+(2b)^2}{12} \approx \frac{(2b)^3 q}{12}. \quad (11)$$

Therefore, $EI_s/GJ_s \approx \bar{q}^2\left(E/G\right)$. If the material is kept the same between the model scale and full-scale, then EI_s/GJ_s scales with $\bar{q}^2$. Next, we observe that $m_s = \rho_s q \cdot 2b$ for a plate with a rectangular cross-section, where ρ_s is the solid mass density. Therefore, $\bar{\mu} = \rho_s/\rho_f$ is just the solid to fluid density ratio.

As defined in Table 1, $\bar{U}$ is the ratio of the inflow speed to the theoretical static-divergence speed (U_{Dt}) of an isotropic hydrofoil with torsional stiffness GJ_s without bend-twist coupling and without warping stiffness effects. The critical static divergence speed is the speed at which the steady-state lift-induced moment about the E.A. is equal to the structural elastic restoring moment (Young, et al. 2018); hence, U_{Dt} is solved using Eqn. (12):

$$\tfrac{1}{2}\rho_f U_{Dt}^2 a_0 (2b) eb\left(\alpha_0 + \psi\right) = K_\psi \psi \ , \quad (12)$$

where

$$K_\psi = \omega_{\psi t0}{}^2 I_s^{E.A.} = \frac{\pi^2 GJ_s}{4L^2} \quad (13)$$

is the torsion stiffness of the plate along E.A. in vacuum, and $\omega_{\psi t0}$ is the 1st torsion frequency of the plate in vacuum (derived through the classical beam torsion model without bend-twist coupling and without warping). Therefore, U_{Dt} is

$$U_{Dt} = \left(\frac{\pi^2 GJ_s}{\rho_f a_0 (2b)^4 AR^2 e}\right)^{1/2}. \quad (14)$$

In this study, we vary $\left\{AR, \bar{q}, \mu, \bar{U}\right\}$ to study their impact on the dynamic hydroelastic response and stability boundaries. Note that it was reported in (Besch & Liu

1974) that different $\bar{\mu}$ values would result in different flutter mechanisms and critical speed limits for isotropic plates. In the results shown next, we non-dimensionalize the frequency ω as

$$\bar{\omega} = \frac{\omega}{\omega_{\psi t}}, \tag{15}$$

where, $\omega_{\psi t}$ is the 1st torsion frequency of the plate in water (derived through the classical beam torsion model without bend-twist coupling and without warping):

$$\omega_{\psi t} = \left(\frac{GJ_s \pi^2}{\rho_s (2b)^6 AR^2 \bar{q} \left(\frac{1}{3} + \frac{\pi}{32 \bar{\mu} \bar{q}} \right)} \right)^{1/2} \tag{16}$$

3. SCALING THE DYNAMIC RESPONSE OF COMPOSITE CANTILEVER PLATES

As shown in (Zarruk et al 2014), (Young et al 2018), (Liao et al 2019), (Akcabay & Young 2019), the elastic response of composite cantilever plates varies with material anisotropy. When the fibers were aligned towards the leading edge (positive θ, as in Fig. 1a), the twist deformations were nose-down and static-divergence was eliminated. Nose-down deformations reduce the effective angle of attack, which in turn reduce the lift and lift-induced moment (Young et al 2018). However, for positive θ, above certain high-speeds, flutter instability became critical (Akcabay& Young 2019). The mechanism of the onset of the flutter instability was shown to be different for vibrating plates in water compared to in air.

For all the results shown next, the reference geometry and material is the one described in (Akcabay & Young 2018), (Akcabay & Young 2019); namely a 0.3 m long, 0.1 m wide, 0.012 m thick, cantilevered composite plate made of unidirectional carbon reinforced fibers embedded in a matrix material. E_1=117.8 GPa, E_2=13.4 GPa, ν_{12}=0.25, G_{12}=3.9 GPa, solid density, ρ_s=1540 kg/m^3. Table A1 in the Appendix lists the dimensional values of the reference divergence spend and the reference 1st torsion mode frequency of the plate in the fluid it is immersed in.

Table 1: The independent nondimensional parameters governing the physical model

Dimensionless Parameter	***Physical Meaning***	***Dimensionless Parameter***	***Physical Meaning***
θ	Fiber angle	$\bar{\mu} = m_s / (\rho_f 2bq)$	Solid to fluid relative mass ratio
$AR = L/2b$	Aspect ratio	a	Eccentricity of the elastic axis from the midchord
$\bar{q} = q/2b$	Thickness to chord ratio	e	Eccentricity of the center of pressure from the elastic axis
EI_s/GJ_s	Bending to torsion stiffness ratio	x_α	Eccentricity of the center of gravity from the elastic axis
$\bar{U} = U_o/U_{Dt}$	Flow speed to reference Divergence speed ratio		

First, in Fig. 3 (for θ=15°) and Fig. 4 (for θ=-15°), where $\bar{q}$ =0.12 and AR=3, we examine the effect of the solid-to-fluid relative mass ratio ($\bar{\mu}$) and flow speed ($\bar{U}$) on the natural frequencies and damping loss factors (η) of the eigenmodes of the plate. The frequencies and damping factors vary with speed because of the dependence of the fluid loads to speed (Eqns. (8-9)). Dimensionally speaking, the frequencies are lower for low $\bar{\mu}$ cases, due to the increased fluid added-mass terms, as they depend on the fluid density. For a similar reason, typical damping values are higher with lower $\bar{\mu}$. For the plate in air (case with $\bar{\mu}$ =1283) for θ=15°, the frequencies of the 1st and 2nd vibration modes tend to converge with higher flow speeds, but the damping of the 1st mode decreases and becomes zero at the flutter speed of $\bar{U}$ =0.65, while the damping of the 2nd mode keeps increasing. The natural frequency and η of the 3rd mode is mostly constant over the same range. For the case of plate in water ($\bar{\mu}$ =1.54) for θ=15°, the natural frequency of the 1st structural mode (1st among the modes that exist in quiescent fluid) decreases with increasing speed; at the same time, a new mode emerges at a speed about $\bar{U}$ =1.34 with an initially high damping factor, but at the flutter speed of $\bar{U}$ =4.3, the damping of this new mode vanishes. Note that excessive stresses and cavitation may prevent the plate from reaching the flutter speed in practice. It should be noted that $\bar{U}$ can be greater than 1 for positive fiber angles, as the bend-twist coupling induces nose-down deformations and hence static-divergence typically does not occur for such plates. Recall that the theoretical divergence speed, U_{Dt}, was derived for an isotropic plate with the same GJ_s but without the bend-twist coupling or warping stiffness terms.

For the case with θ=-15° in Fig. 4, flutter does not occur in air and in water, but the plate undergoes static-

divergence instability at a much reduced flow speed, $\bar{U}$ =0.54 both in air and in water, because of the higher load created by the nose-up deformation for plates with negative θ. Just before the static-divergence, a new mode arises again, both in air and in water, slightly below the 0 vibration frequency, and the damping value of this mode suddenly becomes negative at the critical speed. Notice that static divergence occurred while the structural modes still have a positive frequency for both the plates in air and in water. This type of static divergence can be dangerous, as it can occur without sufficient warning, as it is caused by the new mode.

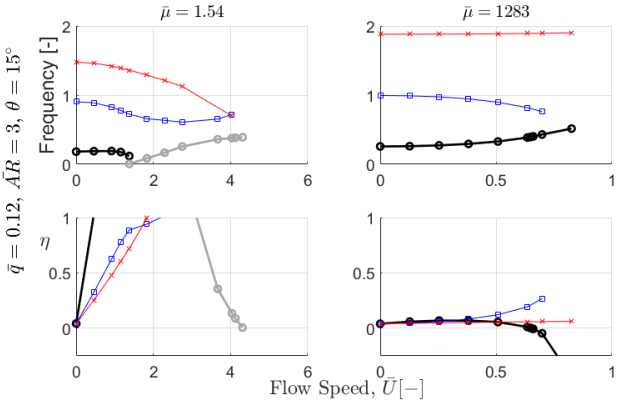

Figure 3: The effect of nondimensional solid-to-fluid density ratio $\bar{\mu}$ and flow speed $\bar{U}$ on the dimensionless natural frequencies and associated damping for fiber angle θ = 15º.

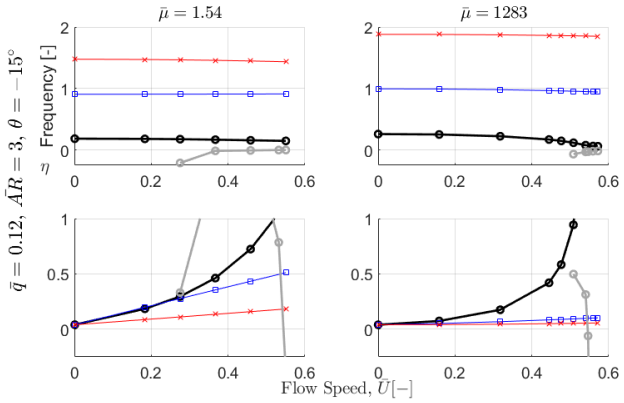

Figure 4: The effect of nondimensional solid-to-fluid density ratio $\bar{\mu}$ and flow speed $\bar{U}$ on the dimensionless natural frequencies and associated damping for fiber angle θ = -15º.

For the plate in water ($\bar{\mu}$ =1.54) and for *AR*=3, Figs. (5) and (6) show the effect of changing the flow speed $\bar{U}$ and $\bar{q}$, the relative thickness of plate, for θ=15º and θ=-15º, respectively. The results with $\bar{q}$ =0.06 and 0.12 are essentially the same; although, dimensionally speaking, the critical speeds and the typical frequencies will be significantly lower with thinner plates (as shown in Table A1 in the Appendix). Our plate model postulates a linear stress gradient across the thickness and our fluid model altogether omits plate thickness effects via the "thin plate" assumption. Therefore, it is intuitive that changing the relative plate thickness would not result in any difference to the nondimensional quantities considered here. The results show that for θ=15º, flutter governs, and for θ=-15º, static divergence governs, and both are caused by the new mode. Also note that for the cases with θ=-15º, the natural frequency of the new mode is very close to zero, and that static divergence again develops while the natural frequencies of the structural modes are still positive.

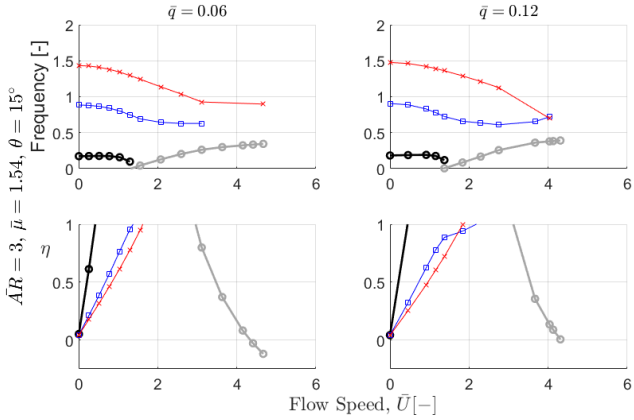

Figure 5: The effect of nondimensional thickness ratio $\bar{q}$ and flow speed $\bar{U}$ on the dimensionless natural frequencies and associated damping for fiber angle θ = 15º and in water.

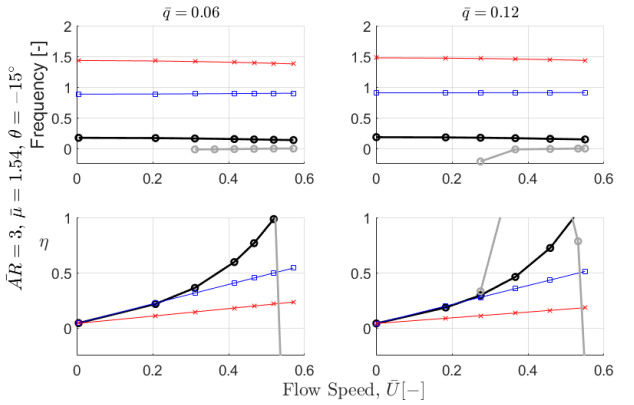

Figure 6: The effect of nondimensional thickness ratio $\bar{q}$ and flow speed $\bar{U}$ on the dimensionless natural frequencies and associated damping for fiber angle θ = -15º and in water.

Figs. (7) and (8) show the effect of changing the flow speed $\bar{U}$ and aspect ratio, *AR*, of the plate in water ($\bar{\mu}$ =1.54), for when $\bar{q}$ =0.12. Dimensionally speaking, as the *AR* increases, the dimensional loads will increase, the natural frequencies will decrease, and the critical speeds will decrease. The nondimensional trends of the behavior for *AR*=3 and 6 are similar, but these responses are different from the response with *AR*=1. This difference is because of reduced downwash effects with higher *AR* (Glauert 1947). In Figs. (7) and (8), note that the reference divergence speed scale used to non-dimensionalize the speed does not account for the warping stiffness effects, which are increasingly important with plates with shorter aspect ratios; hence the reference velocity scale under-predicts divergence speed for short plates. A similar argument holds for the

predicted versus the theoretical reference 1st torsion natural frequency in water. The theoretical divergence speed, U_{Dt}, also does not account for the stiffening (or de-stiffening) due to positive (or negative) bend-twist coupling effects and hence underestimates (or overestimates) the divergence speed for plates with positive (negative) fiber angles. Note that comparison of $\bar{U}$ with *AR* for an isotropic plate (i.e. without bend-twist coupling) but with warping is given in Table A2, both of which converges toward 1.0 with higher *AR*, i.e. as warping effect becomes negligible. Similarly, Table A3 shows the predicted 1st torsion frequency in still fluid converges to the predicted value of 1.0 with higher *AR*, as warping effects becomes negligible.

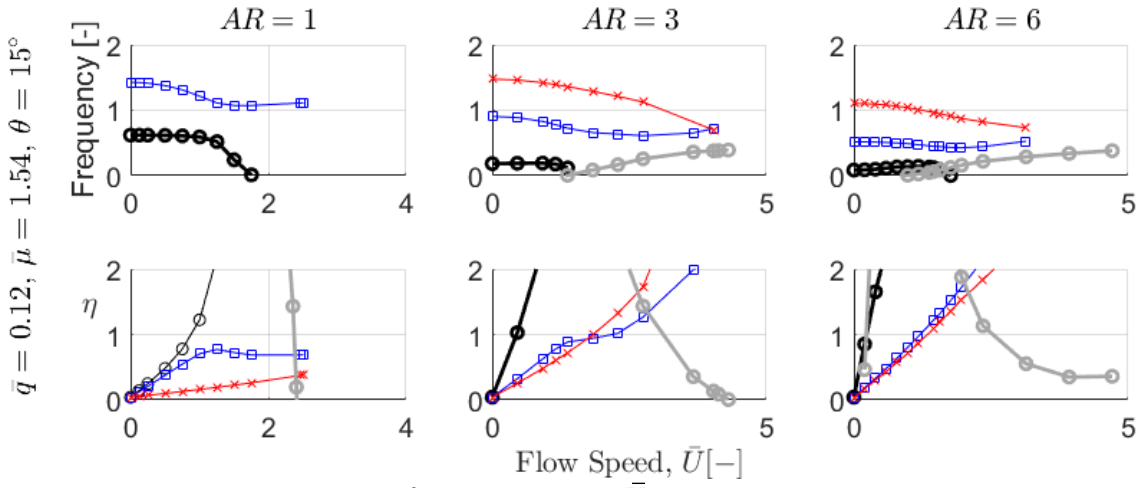

Figure 7: The effect of the aspect ratio AR and flow speed $\bar{U}$ on the dimensionless natural frequencies and associated damping for fiber angle θ = 15º and in water.

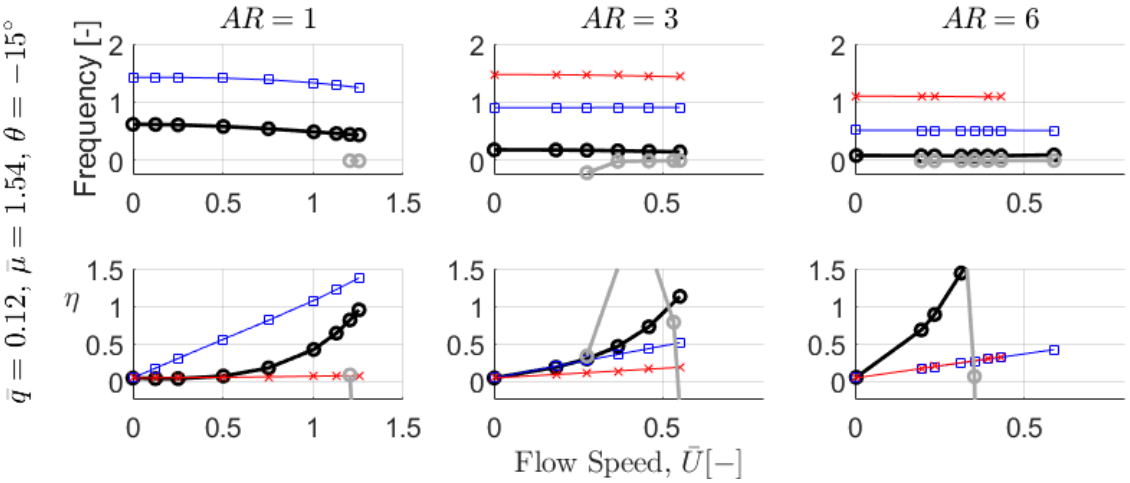

Figure 8: The effect of the aspect ratio AR and flow speed $\bar{U}$ on the dimensionless natural frequencies and associated damping for fiber angle θ = -15º and in water.

4. SUMMARY AND CONCLUSIONS

We have derived the critical nondimensional parameters that govern the dynamic elastic response of composite hydrofoils and airfoils. Specifically, the nondimensional parameters considered include the relative mass ratio, relative velocity ratio, aspect ratio, and thickness-to-chord ratio. We approximated the plate vibrations by coupling a dynamic composite beam model with and an unsteady potential flow model with the 3-D corrections given by (Yates Jr., 1966). The current model ignores the influence of fluid viscosity, free surface, and cavitation.

The results show that the natural frequencies and damping coefficients of hydrofoils and airfoils change with speed because the fluid forcing terms change with speed. For the same composite foil, the in-water natural frequencies tend to be lower, and the damping coefficients tend to be higher, than the in-air values. When the fibers are oriented moderately towards the foil leading edge, bend-up and nose-down deformation results from positive incidence, which tends to decrease the loads relative to the rigid values and static-divergence can be avoided. When the fibers are oriented towards the foil trailing edge, bend-up and nose-up deformation results from positive incidence, which tends to increase the loads relative to the rigid values and promotes static divergence in addition to stall and cavitation.

For composite hydrofoils, a new mode may arise at certain critical speeds, initially with near zero natural frequency and with relatively high damping. For cases in

air and in water where the fiber angle is leaned towards the trailing edge, the natural frequency of this new mode remains very close to zero, and static divergence develops when both the natural frequency and the damping of this new mode go to zero, while the natural frequencies of the structural modes (modes that exist in quiescent fluid) are still positive. This type of static divergence can be dangerous, as it can occur without sufficient warning. For cases in water where the fiber angle is leaned towards the leading edge, at higher speeds, the frequency of this new mode grows and the damping may vanish, resulting in flutter. In contrast, in air, flutter typically occurs when one of the original structural modes of the plate losses its damping at a critical speed. The emergence of the new mode for hydrofoil is caused by the speed dependency and memory effect of the fluid damping and de-stiffening force terms. The new mode can lead to destructive large-amplitude low-frequency vibrations and even flutter at higher speeds. Some of these dynamic results above were also dimensionally discussed in (Akcabay & Young 2019), and the static-divergence results are also in line with the theorertical data given in (Young et al 2018).

Changing the aspect ratio showed that warping stiffness effect played an increasingly bigger role for shorter plates and the critical speeds for hydroelastic instabilities were higher. Dimensionally speaking, normalized lift forces asymptotically increase with longer plates because of reduced downwash effect. The lower lift forces for shorter plates would result in lower deformations, lower flow-induced damping, and higher dimensional critical speed for flutter and static-divergence instabilities. Lowering the thickness to chord ratio lowers the dimensional structural stiffness, resonance frequencies and divergence speed, but the non-dimensional results remain unchanged, as the potential flow model did not account for thickness effects, and the beam model ignored shear effects.

ACKNOWLEDGEMENTS

This work was supported with grants from the Office of Naval Research (ONR), Nos. N00014-16-1-2972 and N00014-18-1-2333 managed by Ms. Kelly Cooper.

APPENDIX

Table A1: List of the dimensional values that are used as the reference speed and frequency in the presented results with θ=±15°. The shaded row is the reference case that has been used in all the comparisons in Figs. (3-8).

$\bar{\mu}$	*AR*	$\bar{q}$	U_{Dt} [m/s]	$\omega_{\psi t}/2\pi$ [Hz]	GJ_s [N.m^2]
1.54	1	0.12	199	980	613
1.54	3	0.12	54.5	327	613
1.54	6	0.12	25.4	163	613
1.54	3	0.06	19.3	128	76.7
1283	3	0.12	1574	525	613

Table A2: Effect of plate aspect ratio (*AR*) on the predicted divergence speed for $\bar{q}$ =0.12, $\bar{\mu}$ =1.54, with GJ_s=224.6 N.m^2 and K_s=0 (i.e. no bend-twist coupling. In the absence of warping stiffness, the divergence speed should be at $\bar{U}$ =1.

AR	$\bar{U}$ at divergence
1	2.69
3	1.48
6	1.23

Table A3: Effect of plate aspect ratio (*AR*) on the predicted 1st torsion natural frequency in still fluid for $\bar{q}$ =0.12, $\bar{\mu}$ =1.54, with GJ_s=224.6 N.m^2 and K_s=0 (i.e. no bend-twist coupling). In the absence of warping stiffness, the 1st torsion frequency should be at $\bar{\omega}$ =1.

AR	$\bar{\omega}$ for 1st torsion in still fluid
1	2.22
3	1.36
6	1.16

BIBLIOGRAPHY

Akcabay, D.T., & Young, Y.L. (2012a). 'Hydroelastic response and energy harvesting potential of flexible piezoelectric beams in viscous flow'. Physics of Fluids, *24*(054106), 1-19.

Akcabay, D.T., & Young, Y.L. (2012b). 'Scaling the dynamic response and energy harvesting potential of piezoelectric beams'. Applied Physics Letters, 101(26): 1-3.

Akcabay, D.T., & Young, Y.L. (2018). 'Influence of material anisotropy on the hydroelastic response of composite plates in water'. Proceedings of SPIE 10596, Behaviour and Mechanics of Multifunctional Materials and Composites XII (pp. 105961M-1 - 105961M-15). Denver, CO, U.S.A.: SPIE.

Akcabay, D.T., & Young, Y.L. (2019). 'Steady and dynamic hydroelastic behavior of composite lifting surfaces'. Composite Structures, in review.

Beaulieu, G., & Noiseux, D. (1981). 'Computation of the modes and polar moment of inertia of the blades of an HAWT'. Proceedings of the wind turbine dynamics workshop, NASA CP-2185, DOE CONF-810226, (pp. 177-186). Cleveland, Ohio, U.S.A.

Besch, P.K., & Liu, Y.-N. (1974). Hydroelastic design of subcavitating and cavitating hydrofoil strut systems. Bethesda, Maryland, U.S.A.: Naval Ship Research and Development Center.

Botelho, E.C., Silva, R.A., Pardini, L.C., & Rezende, M.C. (2006). 'A review on the development and properties of continuous fiber/epoxy/aluminum hybrid composites for aircraft structures'. Materials Research, 9(3): 247-256.

Chen, G.-S., & Dugundji, J. (1987). 'Experimental aeroelastic behavior of froward-swept graphite/epoxy

wings with rigid-body freedom'. Journal of Aircraft, 24(7): 454-464.

Ducoin, A., & Young, Y.L. (2013). 'Scaling of the hydroelastic response of flexible lifting bodies in transitional and turbulent flows'. Proceedings of OMAE ASME Ocean, Offshore and Artic Engineering (pp. V005T06A073-V005T06A073). Nantes, France: American Society of Mechanical Engineers.

Edwards, J.W., & Wieseman, C.D. (2008). 'Flutter and divergence analysis using the generalized aeroelastic analysis method'. Journal of Aircraft, 45(3): 906-915.

Erturk, A., & Inman, D.J. (2011). Piezoelectric energy harvesting. Chichester, West Sussex, U.K.: John Wiley & Sons, Ltd.

Farsadi, T., & Hasbestan, J. (2017). 'Calculation of flutter and dynamic behavior of advanced composite swept wings with tapered cross section in unsteady incompressible flow'. Mechanics of Advanced Materials and Structures, 1-19. doi:10.1080/15376494.2017.1387322

Gay, D., & Hoa, S. V. (2007). Composite Materials, Design and Applications. Second Edition ed.. CRC Press.

Glauert, H. (1947). The elements of aerofoil and airscrew theory. New York, U.S.A.: Cambridge University Press.

Kramer, M. R., & Young, Y. L. (2013). 'Free Vibration of cantilevered composite plates in air and in water'. Composite Structures, 95: 254-263.

Lee, Y.-J., & Lin, C.-C. (2004). 'Optimized design of composite propeller'. Mechanics of advanced materials and structures, 11(1): 17-30.

Liao, Y., Garg, N., Martins, J.R.R.A., & Young, Y.L. (2019). 'Viscous fluid-structure interaction response of composite hydrofoils'. Composite Structures, 212: 571-585.

Lin, J.J. (1996). The coupled hydroelastic behavior of composite marine propellers. Taiwan University. Taiwan: Ph.D. Thesis, Taiwan University.

Lottati, I. (1985). 'Flutter and Divergence Aeroelastic Characteristics for Composite Forward Swept Cantilevered Wing'. Journal of Aircraft, 22(11): 1001-1007.

Mihaila-Andres, M., Larco, C., Rosu, P.-V., & Rotaru, C. (2016). 'Aeroelastic tailoring of composite aircraft wings'. AIP Conference Proceedings, 1863: 420002-1-420002-4. Rhodes, Greece.

Minguet, P. (1989). Static and dynamic behavior of composite helicopter blades under large deflection. Cambridge, MA, U.S.A.: Massachusetts Institute of Technology.

Motley, M.R., & Young, Y.L. (2012). 'Scaling of the transient hydroelastic response and failure mechanisms of self-adaptive composite marine propellers'. International Journal of Rotating Machinery, 2012. doi:10.1155/2012/632856

Sears, W.R. (1941). 'Some Aspects of Non-Stationary Airfoil Theory and Its Practical Application'. Journal Of the Aeronautical Sciences, 8(3): 104-108.

Shirk, M.H., Hertz, T.J., & Weisshaar, T.A. (1986). 'Aeroelastic tailoring - theory, practice, and promise'. Journal of Aircraft, 23(1): 6-18.

Theodorsen, T. (1935). 'General theory of aerodynamic instability and the mechanisms of flutter'. National Advisory Committee for Aeronautics, Report No. 496.

Weisshaar, T.A. (1980). 'Divergence of forward swept composite wings'. Journal of Aircraft, 17(6): 442-448.

Weisshaar, T.A. (1981). 'Aeroelastic tailoring of forward swept composite wings'. *Journal of Aircraft, 18*(8), 669-676.

Weisshaar, T. A., & Foist, B. L. (1985). 'Vibration Tailoring of Advanced Composite Lifting Surfaces'. Journal of Aircraft, 22(2): 141-147.

Yates Jr., E.C. (1966). 'Modified-strip-analysis method for predicting wing flutter at subsonic to hypersonic speeds'. Journal of Aircraft, 3(1): 25-29.

Young, Y. L. (2008). 'Fluid-structure interaction analysis of flexible composite marine propellers'. Journal of Fluids and Structures, 24(6): 799-818.

Young, Y. L., Garg, N., Brandner, P. A., Pearce, B. W., Butler, D., Clarke, D., & Phillips, A. W. (2018). 'Load-dependent bend-twist coupling effects on the steady-state hydroelastic response of composite hydrofoils'. Composite Structures, 189(1): 398-418. doi:10.1016/j.compstruct.2017.09.112

Young, Y. L., Motley, M. R., Barber, R., Chae, E. J., & Garg, N. (2016). 'Adaptive composite marine propulsors and turbines: Progress and challenges'. Applied Mechanics Reviews, 68: 060803-1-34.

Young, Y.L., Harwood, C.M., Montero, F.M., Ward, J.C., & Ceccio, S.L. (2017). 'Ventilation of lifting bodies: review of the physics and discussion of scaling effects'. Applied Mechanics Reviews, 69: 010801.

Zarruk, G. A., Brandner, P. A., Pearce, B. W., & Phillips, A. W. (2014). 'Experimental Study of the Steady State Fluid Structure Interaction of Flexible Hydrofoils'. Journal of Fluids and Structures, 51: 326-343.